Materials Advances

ROYAL SOCIETY OF CHEMISTRY

COMMUNICATION

View Article Online
View Journal | View Issue

Cite this: *Mater. Adv.*, 2024, 5, 1468

Received 7th October 2023,
Accepted 11th January 2024

DOI: 10.1039/d3ma00821e

rsc.li/materials-advances

Photochromic clock reaction of anthraquinone in supramolecular gel and its application to spatiotemporal patterning†

Sota Fujisaki,[a] Yuki Nagai, *[a] Yoshinori Okayasu [a] and Yoichi Kobayashi *[ab]

Nonlinear chemical dynamics observed in clock and oscillating reactions are crucial for understanding non-equilibrium systems and designing sophisticated chemical systems and functional materials. Here, we report anthraquinone-based photochromic gel materials showing a clock reaction-like behavior in the color and fluorescence changes. This unique coloration dynamics results from competition between the photoreduction reaction and inhibition of the reaction by molecular oxygen, which is regulated in the supramolecular gel medium. The induction period until coloration is tunable by the dissolved oxygen concentration and the irradiated light intensity. Spatiotemporal photopatterning based on the photochromic clock behavior was also demonstrated for applications in encryption technologies and display devices.

Nonlinear chemical dynamics are typically observed in clock reactions and oscillating reactions.[1,2] Such chemical reactions have long attracted much attention in chemistry, physics, and life sciences because their behaviors are strongly related to non-equilibrium or dissipative systems.[3–5] Clock reactions are defined as chemical reactions where a product, which has visible color in many examples, is formed in a detectable amount with a well-defined delay (*i.e.*, induction period) after mixing the reactants.[6] Clock reactions are classified into several types in terms of the mechanism, and the most typical one is based on substrate depletion. In this type of clock reaction, sudden coloration occurs after almost complete consumption of certain chemical species like sulfite/thiosulfate (the Landolt reaction)[7,8] and arsenous acid (the Roebuck reaction).[9,10] Although clock behaviors have recently been applied to various functional materials (*e.g.*, for guest release and sensing),[11–14] the versatility of clock reactions is limited because externally adding reactants as a trigger is necessary to start the reaction.

Meanwhile, with respect to the regulation of chemical reactions, photochemical reactions are useful because light provides energy to drive thermodynamically unfavored reactions, and it is also a remote external stimulus with superior spatiotemporal resolution. Among the various photochemical reactions, photochromic reactions, which show reversible color and/or structural changes upon photoirradiation, have attracted the interest of chemists and have been applied to various technologies, such as display devices,[15,16] encryption,[17] energy storage,[18,19] and molecular manipulation.[20,21] In photochemical reactions, if clock behaviors that the desired reaction proceeds with a well-defined induction period after starting photoirradiation are achieved, it leads to the prevention of accidental reaction progress by ambient light and the development of temporally-controlled photofunctional materials and light-fueled dissipative chemical systems.[22–27]

In many cases, photochemical reactions occur *via* triplet excited states with a long lifetime and give radical species as the intermediates. Triplet excited states and radical species are quenched by molecular oxygen, and hence molecular oxygen is usually avoided in photochemical reactions.[28] However, seen from a different perspective, molecular oxygen is a reagent that is easily provided from the air. Moreover, the intentional utilization of quenching by oxygen is expected to result in substrate-depletive clock behaviors in photophysical and photochemical processes *via* triplet excited states and radical species. Actually, photoactivated phosphorescence based on triplet quenching by molecular oxygen in gel or polymer-film matrices has recently attracted increasing attention in applications to encryption technology.[29–31] On the other hand, although clock or sigmoidal dynamics are seen in many photochemical reactions as well,[32,33] such clock behaviors have scarcely been utilized positively in photofunctional materials. This would be due to the difficulty in the oxygen control in solutions and the lack of reversibility.

In this study, we developed a photochromic clock reaction system based on oxygen depletion in a temperature-responsive

[a] *Department of Applied Chemistry, College of Life Sciences, Ritsumeikan University, 1-1-1 Nojihigashi, Kusatsu, Shiga 525-8577, Japan.*
E-mail: ynagai@fc.ritsumei.ac.jp, ykobayas@fc.ritsumei.ac.jp
[b] *PRESTO, JST, 4-1-8 Honcho, Kawaguchi, Saitama 332-0012, Japan*

† Electronic supplementary information (ESI) available: Details of materials, experiments, optical spectra of the solution and gel samples, discussion on the induction period, and movies of the spatiotemporal patterning in the gels with and without NaOH. See DOI: https://doi.org/10.1039/d3ma00821e

supramolecular gel,[34,35] prepared by adding a gelator to ethanol (EtOH) solution of anthraquinone (AQ) and triethylamine (TEA) as the reducing agents (Fig. 1 and 2a).[36] Photoirradiation to the air-saturated gel does not initially lead to photoreduction because the intermediates, including triplet excited states and radical species, are quickly quenched by the dissolved triplet oxygen ($^3O_2$) (Fig. 1c right). Upon quenching, the $^3O_2$ is converted into reactive oxygen species, such as singlet oxygen and superoxide anion, to be consumed mainly *via* reactions with TEA. Once the oxygen concentration is sufficiently decreased after an induction period, the photoreduction and consequent coloration begin to progress rapidly. This coloration is retained for a long time in the gel state because the oxygen penetration from the gas phase based on convective diffusion is suppressed.[37,38] Contrastingly, the heating-induced gel-to-sol transition enables the rapid supply of molecular oxygen from the gas phase, and the reduced form is oxidized to return the sample to the original colorless state. The induction period in photoreduction is tunable by changing the irradiated light intensity and the partial pressure of oxygen in the sample. We also conducted spatiotemporal photopatterning using the photochromic clock reaction to demonstrate the potential of our system in applications such as encryption technology. Our strategy based on oxygen transfer regulation using supramolecular gels can be widely applied to other photochemical reactions *via* triplet excited states and radical species.

Fig. 2b shows the absorption spectra of the air-saturated EtOH gel. AQ exhibited an absorption peak assigned to the π–π* transition at ~320 nm. However, the weak n–π* absorption band, which is observed at ~400 nm in the solution (Fig. S2a, ESI†), was unclear owing to the scattering caused by the gel. After 365-nm LED irradiation, the peak at ~320 nm decreased, and new absorption bands appeared instead. According to the literature, the broad absorption band at 375 nm is attributed to AQH_2, and the weak tail at ~500 nm is to AQH^-, which was partially produced owing to the basicity of TEA.[36] The color of the reduced forms disappeared quickly when the gel-to-sol transition occurred upon heating to 55 °C, and the absorption spectrum was almost recovered after subsequent re-gelation by cooling at room temperature. We consider that convection allowed by the gel–to–sol transition induced the quick oxygen supply from the air to bring the decoloration. Fig. S4 (ESI†) exhibits the fluorescence spectra of the air-saturated gel. The gel showed almost no emission before the LED irradiation, whereas a fluorescence peak resulting from AQH_2 was observed at 470 nm after the LED irradiation.[39] This fluorescence signal disappeared after the sol–gel transition was caused to oxidize the reduced forms.

Fig. 2c displays the coloration dynamics of the gel probed at 400 nm under 365 nm LED irradiation. In the N_2-bubbled gel, the photoreduction progressed immediately after the beginning

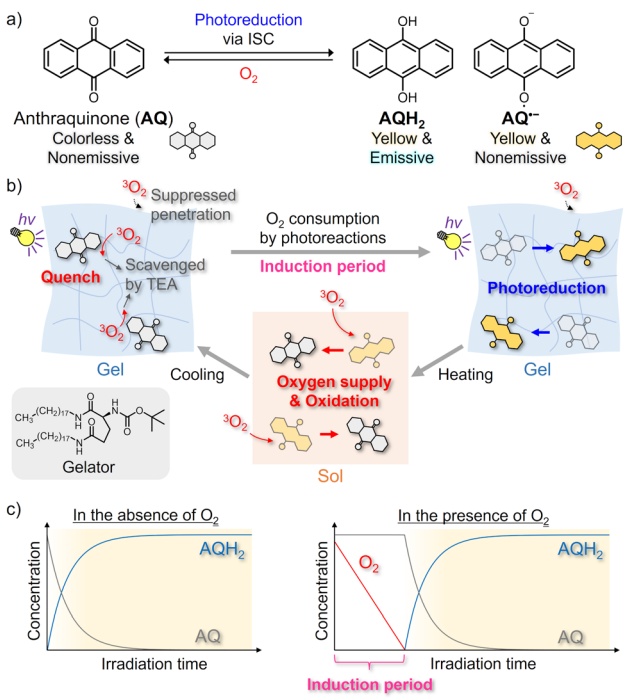

Fig. 1 (a) Photoreduction of anthraquinone (AQ) and oxidation of the reduced forms; (b) Schematic image of the photochromic clock reaction of AQ in the supramolecular gel; (c) Concentration change in the photoreduction of AQ to AQH_2 in the absence (left) and presence (right) of O_2.

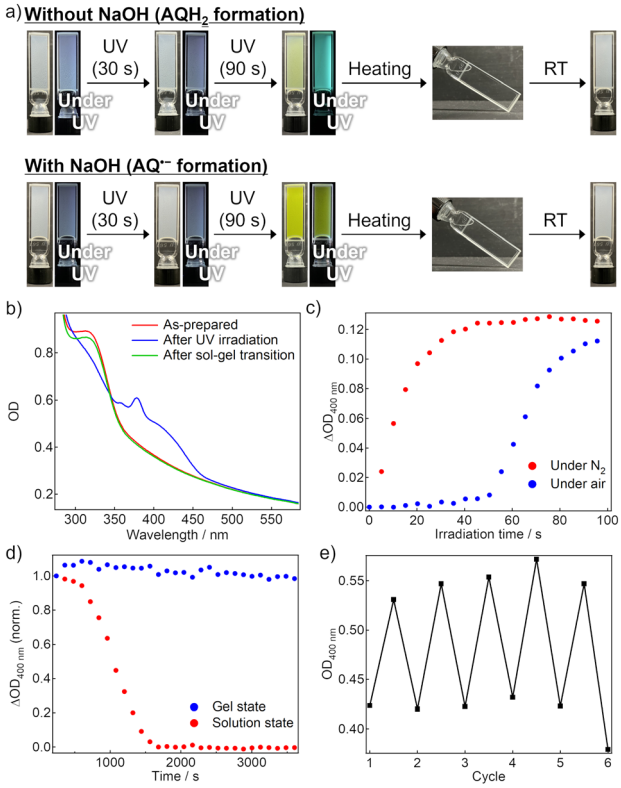

Fig. 2 (a) Images of the AQ gels (top: without NaOH, bottom: with NaOH); (b) Absorption spectra of the gel (400 μM AQ, 4 mM TEA, and no NaOH in EtOH; 1-mm cuvette) before and after UV light irradiation (365 nm, 14.5 mW cm^{-2}) and sol–gel transition; (c) Coloration dynamics at 400 nm for the N_2-bubbled and air-saturated gels upon continuous UV light irradiation; (d) Coloration decay at 400 nm for the gel and solution after UV light irradiation; (e) Cyclability of photoreduction and air-oxidation of the gel.

of photoirradiation, while a clock behavior was observed in the LED irradiation to the air-saturated gel; an induction period of ~50 s was observed until the visible absorption started to rise owing to the formation of the reduced forms. The slight increase in the optical density (OD) during the induction period was not due to photoreduction but caused by scattering increase. We considered that the dissolved oxygen was consumed during the induction period to trigger significant progress of the photoreduction. Such clock behavior was also observed in the air-saturated EtOH solution (Fig. S2c, ESI†), and even in the air-saturated methanol solution and gel (Fig. S12 and S13, ESI†). These results show that the clock behaviors are neither brought by the gelation nor by just the presence of EtOH.

Unlike the gel without NaOH, 365 nm LED light irradiation to the air-saturated EtOH gel with added NaOH resulted in the formation of new absorption bands in the visible and near-infrared region owing to the generation of $AQ^{\bullet-}$ (Fig. 2a bottom and Fig. S5a, ESI†).[36] When heating induced the gel-to-sol transition and thereby the oxygen in the air was supplied to the sample, the absorption spectrum returned to the original shape. In the air-saturated gel, the induction period of ~60 s until the coloration was observed (Fig. S5b, ESI†). $AQ^{\bullet-}$ did not display any detectable emission signals in the air-saturated gel.

We compared the stability of the coloration after photoirradiation between the air-saturated solution and gel (Fig. 2d). In the solution, the absorption of the reduced forms gradually decreased and disappeared almost completely within 30 min. This decoloration was driven by oxygen supply from the air through convective diffusion and molecular diffusion. We note that the decoloration dynamics fluctuated in every measurement because of the natural convection behavior. However, in the gel, the coloration was retained for at least a few hours in the probed area because the oxygen penetration occurred only *via* molecular diffusion from the gas-gel interface.[40] We also evaluated the cyclability of the photoreduction by repeating 365-nm LED irradiation to the air-saturated gel and the sol–gel transition (Fig. 2e and Fig. S7, ESI†). The photoreduction progressed even in the 5th cycle to almost the same degree as the 1st cycle, and hence the cyclability was found to some extent. These results show that the oxygen supply regulation using supramolecular gel is efficient for reversible control of the photoreduction.

If the induction period corresponds to the consumption of the dissolved oxygen, it is expected to be controlled by adjusting the amount of dissolved oxygen. Therefore, we mixed the air and N_2 gas in different volume ratios, and the mixed gases were used for bubbling into the sol state of the gel sample. In the mixed gases, the volume fraction of O_2 changes according to their own Air/N_2 ratio, and thereby the dissolved oxygen concentration is tunable. Fig. 3a shows the coloration dynamics of the gel saturated with different composition gasses under 365-nm LED irradiation. As the fraction of the air (*i.e.*, the fraction of O_2) increased, the induction period was elongated. The length exhibited a linear relationship with the expected volume fraction of O_2, which was calculated assuming that the volume fraction of O_2 in the air is 0.21 (Fig. 3b). This result indicates that the dissolved oxygen concentration determines the duration of the induction period directly.

We also traced the coloration dynamics of the air-saturated gel under 365-nm LED irradiation with different intensities (Fig. S8a–e, ESI†). As the light intensity increased, the induction period decreased, and the subsequent coloration was faster. When the horizontal axis was corrected to the total amount of the irradiated photons, there were overlapping dynamics in each condition (Fig. S8f, ESI†). In Fig. 3c, the induction periods are plotted against the reciprocal number of the irradiated light intensity, clearly indicating a linear relationship. This agrees with our hypothesis that the induction period is dominated by the dissolved oxygen amount.

Furthermore, transient absorption spectroscopy revealed that the dissolved oxygen quenches probably the T_1 state of AQ, the triplet exciplex with TEA, and the radical-ion pair $AQ^{\bullet-}$–$TEA^{\bullet+}$ in our experimental condition (Fig. S9 and S10, ESI†).[36] Importantly, the quenching occurred even in the low oxygen concentration, which indicates that practically, coloration by photoreduction progresses after the dissolved oxygen is almost finished. The relationship between the induction period t_i, the initial concentration of the dissolved triplet oxygen $[^3O_2]_0$, the irradiation light intensity I, and the absorbance of AQ A was approximately given as follows:

$$t_i = \frac{K \cdot [^3O_2]_0}{I \cdot (1 - 10^{-A})} \quad (1)$$

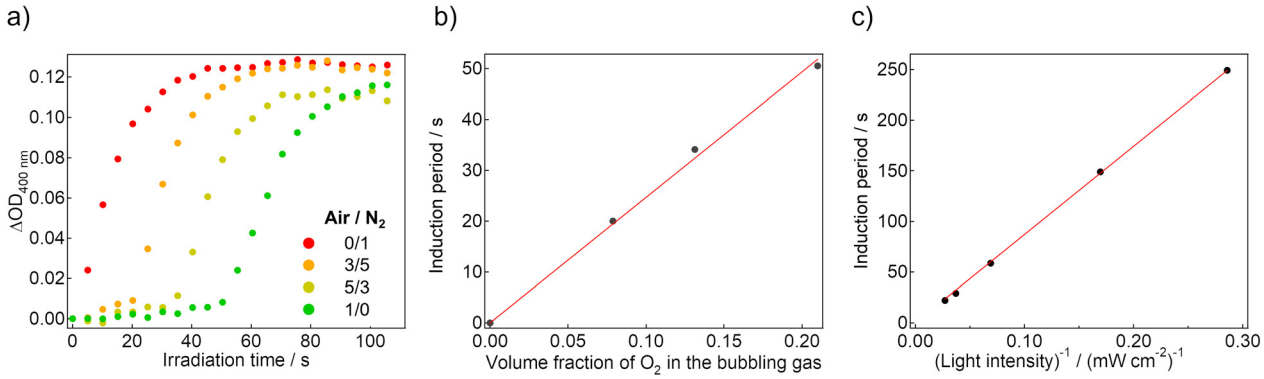

Fig. 3 (a) Coloration dynamics in the gel saturated with different composition gases upon continuous UV light irradiation; (b) Relationship between the induction period and gas composition; (c) Relationship between the induction period and irradiation light intensity.

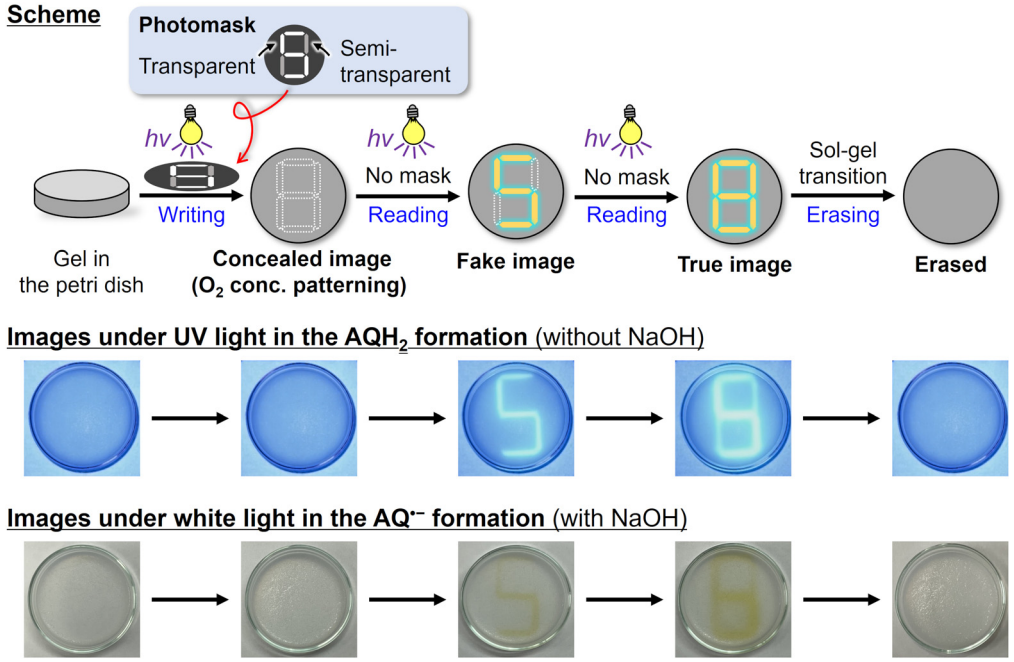

Fig. 4 Spatiotemporal photopatterning experiments; (top) Experimental scheme, (middle) Images under UV light in the condition without NaOH, (bottom) Images under white light in the condition with NaOH.

where K is a constant determined by the experimental condition (See ESI† for details).

Finally, we conducted spatiotemporal patterning and on-demand erasing of the photochromic reaction (Fig. 4, movies in ESI†). We irradiated 365 nm LED light to the air-saturated ethanol gel without NaOH through a photomask having transparent, semi-transparent, and non-transparent parts. After the photoirradiation, there were not yet any reduced forms of AQ, but the information was recorded as the O_2 concentration pattern; the concentration was relatively low under the transparent part, medium under the semi-transparent part, and high under the non-transparent part. In the reading process, we irradiated 365 nm LED light without photomasks. First, the photoreduction proceeded in the low O_2 concentration area to give a fluorescence pattern. Subsequent irradiation causes the photoreduction in the medium concentration area to show another fluorescence pattern. The recorded patterns were erased by the sol–gel transition. Contrastingly, in the condition with NaOH, patterning with intense coloration was obtained instead of fluorescence (Fig. 4, bottom). Although spatiotemporal patterning using photoactivated phosphorescence materials has been reported recently,[29–31,41] this work provides the first example where not only emission but also absorption are spatiotemporally controlled based on photochemical reactions, as far as we know. Such spatiotemporal patterning is promising for applications including encryption technologies and display devices.

Conclusions

We developed a photochromic clock reaction system based on the photoreduction of AQ using a supramolecular gel. Under photoirradiation, an induction period is observed before the photoreduction begins, and this behavior results from the quenching of the triplet excitons and radical-ion pair by molecular oxygen and consequent oxygen consumption. The photoreduction changes the nonemissive colorless state to the blue-emissive yellow state or the nonemissive yellow state depending on the basicity of the gel, and oxygen supplied from the air upon the heating-induced sol–gel transition returns the yellow state to the original colorless state. The duration of the induction period can be controlled by the dissolved oxygen concentration and the irradiated light intensity. In addition, we demonstrated that the photochromic clock reaction is useful for spatiotemporal photopatterning toward applications such as photoresponsive encryption and display devices. Our methodology based on oxygen control using supramolecular gels might be applied to other photochemical reactions relating to triplet excitons and radicals, and contributes to the development of novel photofunctional materials.

Author contributions

S. F: data curation, investigation, validation, visualization, writing – original draft, writing – review & editing. Y. N: conceptualization, data curation, funding acquisition, investigation, resources, software, supervision, visualization, writing – original draft, writing – review & editing. Y. O.: supervision, writing – review & editing. Y. K.: funding acquisition, project administration, resources, supervision, writing – review & editing.

Conflicts of interest

There are no conflicts to declare.

Acknowledgements

This work was supported by JST, PRESTO Grant Numbers JPMJPR22N6, JSPS KAKENHI Grant Numbers JP21K05012, and the Sasakawa Scientific Research Grant from The Japan Science Society.

Notes and references

1 Y. Ding, C. M. Gutiérrez-Ariza, C. Ignacio Sainz-Díaz, J. H. E. Cartwright and S. S. S. Cardoso, *Angew. Chem., Int. Ed.*, 2019, **58**, 6207–6213.
2 A. Molla and J. H. Youk, *Dyes Pigm.*, 2022, **202**, 110237.
3 I. R. Epstein and K. Showalter, *J. Phys. Chem.*, 1996, **100**, 13132–13147.
4 A. S. Mikhailov and K. Showalter, *Phys. Rep.*, 2006, **425**, 79–194.
5 H. W. H. Van Roekel, B. J. H. M. Rosier, L. H. H. Meijer, P. A. J. Hilbers, A. J. Markvoort, W. T. S. Huck and T. F. A. De Greef, *Chem. Soc. Rev.*, 2015, **44**, 7465–7483.
6 A. K. Horváth and I. Nagypál, *Chem. Phys. Chem.*, 2015, **16**, 588–594.
7 J. A. Church and S. A. Dreskin, *J. Phys. Chem.*, 1968, **72**, 1387–1390.
8 D. Varga, I. Nagypál and A. K. Horváth, *J. Phys. Chem. A*, 2010, **114**, 5752–5758.
9 J. R. Roebuck, *J. Phys. Chem.*, 1902, **6**, 365–398.
10 L. Valkai and A. K. Horváth, *Inorg. Chem.*, 2016, **55**, 1595–1603.
11 S. Angelos, N. M. Khashab, Y.-W. Yang, A. Trabolsi, H. A. Khatib, J. F. Stoddart and J. I. Zink, *J. Am. Chem. Soc.*, 2009, **131**, 12912–12914.
12 L. Zheng, H. Yu, Y. Yue, F. Wu and Y. He, *ACS Appl. Mater. Interfaces*, 2017, **9**, 11798–11802.
13 N. Német, G. Holló, G. Schuszter, D. Horváth, Á. Tóth, F. Rossi and I. Lagzi, *Chem. Commun.*, 2022, **58**, 5777–5780.
14 T. Zheng, W. Nie, L. Yu, J. Shu, Y. Li, C. Tian, W. Wang and H. Cui, *Proc. Natl. Acad. Sci. U. S. A.*, 2022, **119**, 1–8.
15 N. Ishii, T. Kato and J. Abe, *Sci. Rep.*, 2012, **2**, 819.
16 Y. Kobayashi and J. Abe, *Adv. Opt. Mater.*, 2016, **4**, 1354–1357.
17 A. Abdollahi, H. Roghani-Mamaqani, B. Razavi and M. Salami-Kalajahi, *ACS Nano*, 2020, **14**, 14417–14492.
18 Q. Qiu, Y. Shi and G. G. D. Han, *J. Mater. Chem. C*, 2021, **9**, 11444–11463.
19 Z. Wang, H. Hölzel and K. Moth-Poulsen, *Chem. Soc. Rev.*, 2022, **51**, 7313–7326.
20 M. Irie, T. Fukaminato, K. Matsuda and S. Kobatake, *Chem. Rev.*, 2014, **114**, 12174–12277.
21 L. Wang and Q. Li, *Chem. Soc. Rev.*, 2018, **47**, 1044–1097.
22 T. Ikegami, Y. Kageyama, K. Obara and S. Takeda, *Angew. Chem., Int. Ed.*, 2016, **55**, 8239–8243.
23 K. Kumar, C. Knie, D. Bléger, M. A. Peletier, H. Friedrich, S. Hecht, D. J. Broer, M. G. Debije and A. P. H. J. Schenning, *Nat. Commun.*, 2016, **7**, 11975.
24 F. Nicoli, M. Curcio, M. Tranfić Bakić, E. Paltrinieri, S. Silvi, M. Baroncini and A. Credi, *J. Am. Chem. Soc.*, 2022, **144**, 10180–10185.
25 S. Corra, M. T. Bakić, J. Groppi, M. Baroncini, S. Silvi, E. Penocchio, M. Esposito and A. Credi, *Nat. Nanotechnol.*, 2022, **17**, 746–751.
26 X. Yang, W. Shi, Z. Chen, M. Du, S. Xiao, S. Qu and C. Li, *Adv. Funct. Mater.*, 2023, 2214394.
27 É. Bartus, A. Tököli, B. Mag, Á. Bajcsi, G. Kecskeméti, E. Wéber, Z. Kele, G. Fenteany and T. A. Martinek, *J. Am. Chem. Soc.*, 2023, **145**, 13371–13383.
28 B. Maiti, A. Abramov, R. Pérez-Ruiz and D. D. Díaz, *Acc. Chem. Res.*, 2019, **52**, 1865–1876.
29 S. Wan and W. Lu, *Angew. Chem., Int. Ed.*, 2017, **56**, 1784–1788.
30 H. Ding, Y. Sun, M. Tang, J. Wen, S. Yue, Y. Peng, F. Li, L. Zheng, S. Wang, Y. Shi and Q. Cao, *Chem. Sci.*, 2023, **14**, 4633–4640.
31 S. Xiong, Y. Xiong, D. Wang, Y. Pan, K. Chen, Z. Zhao, D. Wang and B. Z. Tang, *Adv. Mater.*, 2023, **2301874**, 1–10.
32 C. A. Jones, L. E. Weaner and R. A. Mackay, *J. Phys. Chem.*, 1980, **84**, 1495–1500.
33 C. Decker and A. D. Jenkins, *Macromolecules*, 1985, **18**, 1241–1244.
34 Y. Li, T. Wang and M. Liu, *Soft Matter*, 2007, **3**, 1312–1317.
35 P. Duan, N. Yanai, H. Nagatomi and N. Kimizuka, *J. Am. Chem. Soc.*, 2015, **137**, 1887–1894.
36 K. Hamanoue, T. Nakayama, Y. Yamamoto, K. Sawada, Y. Yuhara and H. Teranishi, *Bull. Chem. Soc. Jpn.*, 1988, **61**, 1121–1129.
37 T. Shoji, N. Katakura, N. Mochizuki, H. Shiroishi and M. Kaneko, *J. Photochem. Photobiol. A Chem.*, 2004, **161**, 119–124.
38 H. Ueno, N. Gokan, Y. Nakano and M. Kaneko, *Bull. Chem. Soc. Jpn.*, 2008, **81**, 1657–1662.
39 S. A. Carlson and D. M. Hercules, *Photochem. Photobiol.*, 1973, **17**, 123–131.
40 Y. Elsayed, C. Lekakou and P. Tomlins, *Polym. Test.*, 2014, **40**, 106–115.
41 P. She, J. Lu, Y. Qin, F. Li, J. Wei, Y. Ma, W. Wang, S. Liu, W. Huang and Q. Zhao, *Cell Rep. Phys. Sci.*, 2021, **2**, 100505.